Instantaneous Response and Mutual Interaction between Wind Turbine and Flow

Andersen, Søren Juhl; Sørensen, Jens Nørkær

Published in:
Journal of Physics: Conference Series

Link to article, DOI:
10.1088/1742-6596/1037/7/072011

Publication date:
2018

Document Version
Publisher's PDF, also known as Version of record

Instantaneous Response and Mutual Interaction between Wind Turbine and Flow

IOP Conf. Series: Journal of Physics: Conf. Series **1037** (2018) 072011 doi:10.1088/1742-6596/1037/7/072011

Instantaneous Response and Mutual Interaction between Wind Turbine and Flow.

Søren Juhl Andersen[1a] **and Jens Nørkær Sørensen**[1]

[1] DTU Wind Energy, Technical University of Denmark, 2800 Lyngby, Denmark.

E-mail: [a]sjan@dtu.dk

Abstract. The mutual fluid-structure interaction between wind turbine(s) and the highly turbulent flow deep inside a large wind farm is investigated in order to elucidate on how to implement and perform dynamic wind farm control. The study employs a fully coupled LES and aeroelastic framework, which provide time resolved flow and turbine response governed by a controller. The results show a large correlation between incoming flow and turbine response, which extends several radii upstream and could be utilized for turbine control by *e.g.* installing a lidar on top of the wind turbine. Similarly, the results are valuable for utilizing nacelle mounted lidars for power curve assessments in large wind farms. However, the correlations between turbine and wake flow as well as the dynamic wake position are low, which is potentially discouraging for attempts to do instantaneous yaw steering.

1. Introduction

The incoming wind affects the performance and loads of an operating wind turbine and similarly the presence of a wind turbine affects the flow as the wind approaches the turbine through the induction zone. Recent studies of these changes to the incoming wind in the induction zone comprise steady state consideration by Troldborg and Forsting [1] and the change in the low frequency part of the spectra by Mann et al. [2].

The flow after the turbine is dominated by the wake, which has been studied extensively, see *e.g.* the engineering model by Jensen [3], experimental study by Bastankhah and Porté-Agel [4], or detailed numerical investigation on the wake structure and breakdown by Sørensen et al. [5].

The wake effects are particularly important when wind turbines are clustered in large wind farms, and hence another active area of research investigates wind farm control to mitigate the unfavorable wake effects and to optimize the performance of wind farms, *e.g.* increase power production and decrease loads. Two main approaches are being investigated for such wind farm control, *i.e.*:

- Induction based control, where essentially the wind turbine thrust is altered to improve farm performance by decreasing the wake effect, *e.g.* Steinbuch et al. [6] and Annoni et al. [7].
- Wake steering, which aims to deflect the wake sufficiently to improve the performance of the next turbine, *e.g.* Gebraad et al. [8] and Fleming et al. [9]

The aforementioned studies have generally focussed on the changes to the flow, often from steady state or at least static operating conditions. Dynamic control of large wind farms has

recently been investigated in detail by Goit and Meyers [10] and subsequently a derived simpler and practical control strategy by Munters and Meyers [11], although the dynamic analysis does not include the effect on the turbine load.

This study investigates the instanteneous and mutual fluid-structure interaction between flow and turbines deep inside large wind farms to address how correlated the turbine response is to the turbulent inflow and, inversely, how does the incoming turbulence change due to the turbine response. The dynamic interaction is important to enable actual wind turbine and wind farm control subject to highly dynamic and complex wake inflow. This interaction is investigated numerically using a fully coupled Large Eddy Simulations (LES) and aeroelastic framework to elucidate on how detailed and how to approach dynamic control in practice.

2. Methodology

Several large wind farms have been modelled using the incompressible finite volume code, EllipSys3D, as developed at DTU and the former Risø, see Michelsen [12] and Sørensen [13]. In the present work the flow is modelled using Ellipsys3D to perform LES. The turbines are modelled with the actuator line method, see Sørensen and Shen [14]. The actuator lines are fully coupled to the aero-elastic code Flex5, see Øye [15]). The coupling yields the full aero-elastic response of the turbine to the incoming turbulent flow, *i.e.* loads and actual blade deflections, which means the actuator lines are also deflected in the flow. See Sørensen et al. [5] for details on the coupling. Furthermore, the aero-elastic framework includes an active controller comprised of a variable speed P-controller for below rated wind speeds and a PI-pitch angle controller for above rated wind speeds.

The turbine is the NM80 turbine, proprietary to Vestas Wind Systems A/S, see Madsen et al. [16]. The employed version of the NM80 is rated to 2.75MW at $U_{hub} = 14$m/s and with $R = 40$m.

Several simulations and statistics of the simulations have previously been presented in Andersen et al. [17], but in the present work the focus is on a simulation with a freestream velocity of 8m/s, a total of 16 turbines in a row with a streamwise turbine spacing of $S_X = 12R$, and turbulence intensity of approximately 15%. The atmospheric boundary layer have been modelled as a combination of a parabolic and power law profile with a shear exponent of $\alpha_{PBL} = 0.14$ using body forces, see Mikkelsen et al. [18] and Troldborg et al. [19] for detail.

Stochastically generated Mann turbulence (Mann [20], [21]) is introduced into the flow upstream of the first turbine using body forces. The influence of the incoming turbulence is deemed minor in the present case as the analysis will focus on turbines operating deep inside the wind farm, where the turbine generated turbulence is dominant. Deep inside the wind farm, the free stream turbulence intensity tends to govern the amount energy entrainment and hence the mean wind speed, while the large atmospheric turbulence length scales are broken down to scales related to the wind turbine spacing as shown by Andersen et al. [22].

Figure 1 shows the domain setup, which is $200R \times 20R \times 20R$ in streamwise (X), lateral (Y), and vertical directions (Z), respectively. Each actuator line (blade) is resolved by 17 cells. 16 turbines are indicated in the figure and the streamwise velocity is shown in two vertical planes, a streamwise and a lateral plane.

3. Results

The mutual interaction between flow and turbine(s) are analysed in two ways, but both approaches rely on the cross-correlation. The cross-correlation (ρ) between two signals (P_1 and P_2) is calculated by:

$$\rho(\tau) = \frac{\sum_i^N [(P_1(t_i) - \overline{P}_1)(P_2(t_i - \tau) - \overline{P}_2)]}{\sigma(P_1) \cdot \sigma(P_2)}$$

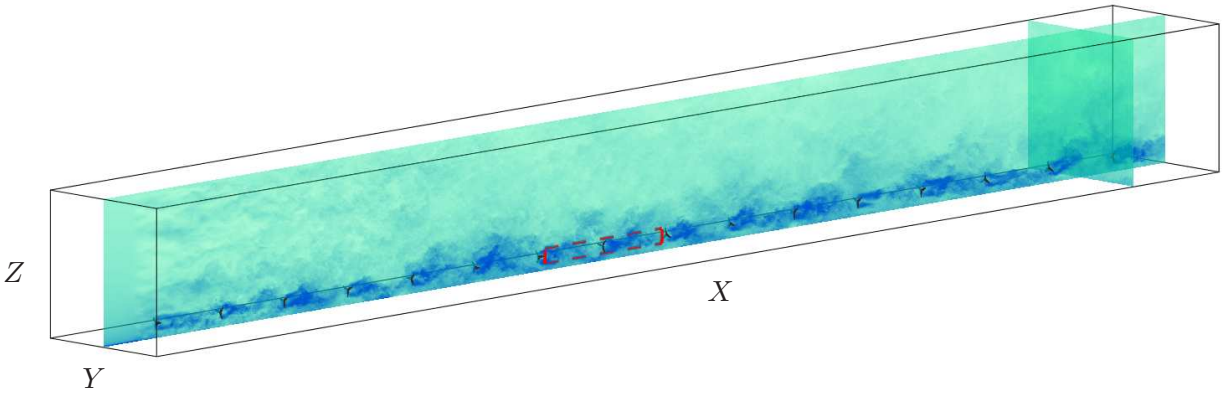

Figure 1. Instantaneous snapshot of the flow and computational domain containing 16 wind turbines with a spacing of 12R. Streamwise velocity contours on streamwise and lateral slices. Red square indicate area used for induction study.

where τ is the time lag and σ the standard deviation. The maximum cross-correlation is a measure of the similarity in the two signal, so a high cross-correlation indicates that flow and turbine response are directly linked. Furthermore, the maximum correlation also yields a corresponding time lag or delay between the two signals.

3.1. Wind Turbine and Flow

The flow is correlated directly to the operation of a wind turbine, *i.e.* the cross-correlation is computed between the streamwise velocity in a point and a given turbine signal, *e.g.* power, thrust, and loading.

Figure 2 shows examples of timeseries of streamwise velocity extracted $1R$ upstream, power production, and thrust force on the 13th rotor. Clearly, the signals are correlated, *e.g.* the power production follows the streamwise velocity. The effect of spatial and temporal filtering is also evident in the power signal. Although the signals are correlated, there is also a shift in the response between power production and the thrust force, *i.e.* the peaks in thrust occurs prior to the peaks in power due to inertia in the generator and the time scale of the turbine controller.

The streamwise velocity is extracted in vertical planes through the rotor centers along the streamwise direction as shown in Figure 1. The temporal correlation is computed between the velocity field in each mesh point relative to the power production and loads on the nearest turbine, *i.e.* both in the upstream induction zone and downstream wake as indicated with the red square in Figure 1.

Cross-correlations have been calculated for the 6th to 14th turbine for ten different 10min periods (total of 100min) separated by approximately 30s with a temporal discretization of 0.2s. The maximum correlation has been determined and the resulting 10×9 correlations matrices for wind turbine operation deep inside wind farms have been ensemble averaged. Figures 3 and 4 shows contour plots of the ensemble averaged correlation between the streamwise velocity and power and thrust force, respectively.

The ensemble averaged correlation between the streamwise velocity and both power and thrust force are as expected very similar and quite symmetric. The mean ensemble averaged correlation are high as it reaches values of approximately $0.7-0.8$, which demonstrate the mutual interaction between the thrust force and the flow, *i.e.* an increased thrust force increase the induction affecting and decreasing the flow velocity, which again leads to a decrease in thrust force. It is also clear how power and thrust are integral quantities over the entire rotor as it is

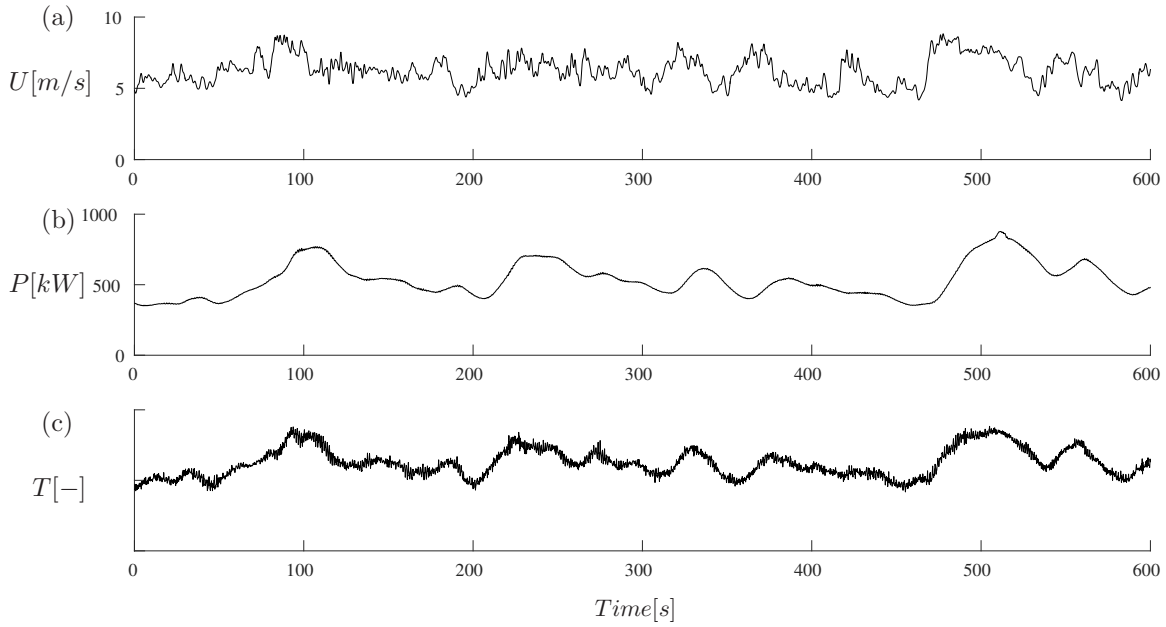

Figure 2. Time series of (a) streamwise velocity extracted $1R$ upstream, (b) power production, and (c) thrust force for the 13th turbine.

centered around hub height. The highly correlated region is larger for the thrust force compared to the power, which relates to the majority of the power being produced on the outer parts of the blades.

The upstream extent of the highly correlated region is important for several applications. A nacelle mounted lidar can be installed to measure the incoming wind to improve power curve assessment, see *e.g.* Borraccino [23], where these results are particular relevant for power curve assessment inside wind farms. The nacelle mounted lidar measurements would also be influenced by the movements of the turbine, which potentially should be corrected for, particular as turbines get larger. Similarly, a nacelle mounted lidar could be used for control purposes by providing inflow measurements directly to the turbine controller. However, the lidar needs to measure a representative inflow in both applications.

For control application, it needs to measure far enough upstream for the controller to have sufficient time to adjust before the wind actually hits the turbine, and at the same time the measurement has to be correlated enough with the actual flow which eventually will hit the turbine to provide accurate control. The ensemble averaged time delay corresponding to the maximum cross-correlation is shown in Figure 5 and of particular interest in terms of control. The time delay is clearly related to the upstream distance. The spacing between the vertical fronts is consistent and yields and estimate of the wake propagation velocity of approximately 6.9m/s.

Hence, the two figures not only give the best location to measure, but also the governing time scale. So a nacelle mounted lidar measuring the incoming wind at *e.g.* $2R$ upstream the turbine would on average give input to the controller with 70% or higher accuracy (not considering the spatial filtering a lidar would employ) and the controller would have approximately 12s to respond and adjust the turbine. Controlling and adjusting the turbine would naturally result in a changed inflow conditions.

The highly correlated regions for both power and thrust force also extend behind the rotor, indicating a slightly delayed response due to inertia, deflections and/or time scales of the controller. The time delay is also clear in Figure 6, which shows the average correlation for flow and the tilting moment. It reaches a maximum contour of 0.3 around the top of the turbine. The location of the highest correlation is expected as a high or low streamwise velocity at the top will influence the tilting moment more than a comparable high or low streamwise velocity at the bottom of the rotor. However, the correlation between the turbine performance and the wake flow is limited. It reaches a minimum approximately $2R$ downstream, which is related to the breakdown of the near wake. The low correlation between the instantaneous response of the turbine and the wake flow appears discouraging for wake steering. On the other hand, it could be advantageous for inducation based control strategies. An induction based control strategy essential aims at reducing the wake deficit, usually by downregulating a turbine. This can be achieved in a number of different ways, see Mirzaei et al. [24]. A control strategy, which triggers a faster breakdown, *e.g.* observed by moving the minimum correlation region even closer to the turbine, would lead to faster wake recovery. Hence, improved performance of the following turbine.

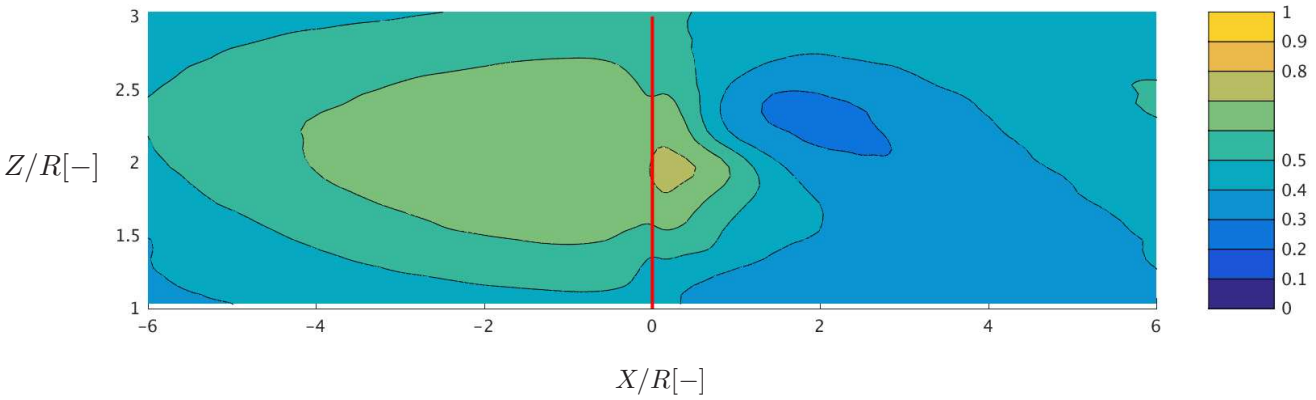

Figure 3. Contours of the ensemble average of the maximum cross-correlation between streamwise velocity and power. Vertical red line indicates turbine.

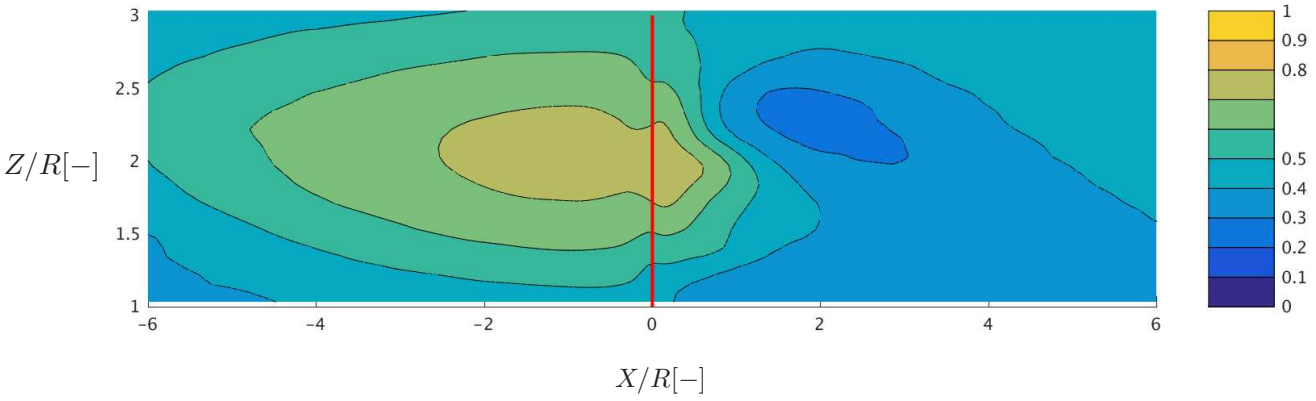

Figure 4. Contours of the ensemble average of the maximum cross-correlation between streamwise velocity and thrust. Vertical red line indicates turbine.

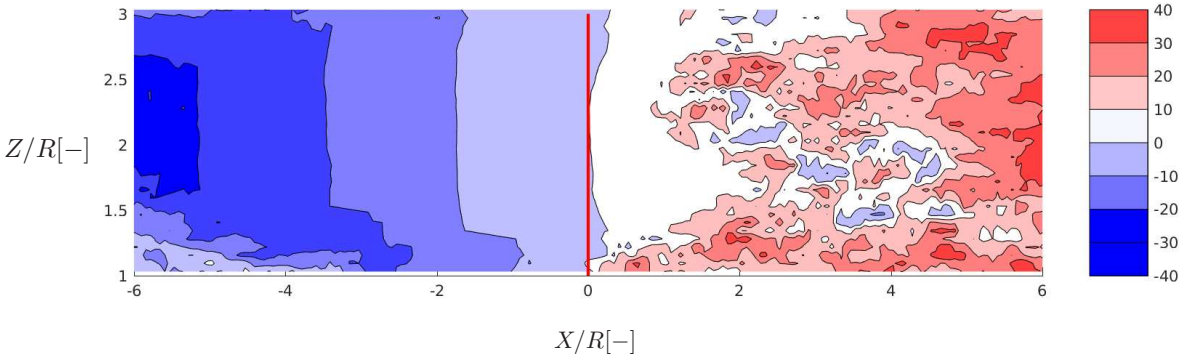

Figure 5. Contours of the ensemble average of the time delay for the maximum cross-correlation of the streamwise velocity and thrust. Vertical red line indicates turbine.

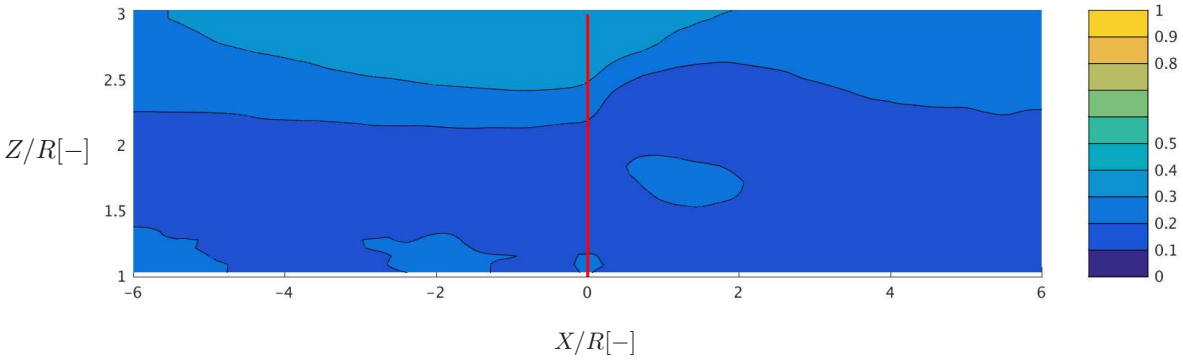

Figure 6. Contours of the ensemble average of the maximum cross-correlation between streamwise velocity and tilting moment. Vertical red line indicates turbine.

3.2. Wind Turbine and Wake Position

Wake steering aims to deflect the wake, so the key is to be able to control the wake position. As previously stated, the correlation between the wake flow and the instantaneous turbine performance and loads is limited, hence the aim here is to investigate the correlation between the turbine and the wake as an coherent entity. Therefore, the center of the wake (Y_C, Z_C) is determined through a center of mass analogy applied to the wake deficit in lateral planes as defined in Figure 1.

The center of the wake is determined iteratively as the wake center coordinate relative to the hub location is updated as $Y_C = Y_C + \Delta Y$ until $\Delta Y < 10^{-3}R$. Similarly for Z_C. ΔY and ΔZ are the changes in center position found through the iteration process by:

$$\Delta Y = \frac{\int (Y - Y_C)(1 - \frac{U}{U_0})^m dA}{\int (1 - \frac{U}{U_0})^m dA}, \qquad \Delta Z = \frac{\int (Z - Z_C)(1 - \frac{U}{U_0})^m dA}{\int (1 - \frac{U}{U_0})^m dA} \tag{1}$$

where dA is the area of each cell in the mesh and the weight has been set to $m = 3$, similar to Andersen [25]. The center position is determined within an area around the hub of $Y = \pm 3R$ and $Z = \pm 1.7R$. The difference in extend is due to the ground. An example of the determined wake center is illustrated in Figure 7. The dynamics of the instantaneous wake are clearly visible and the wake is clearly non-gaussian. Furthermore, the effect of multiple turbines is also seen with

the remants of an additional wake on the right hand side. Hence, the location of the wake center is not indisputable, but the present method generally provides consistent results. Occasionally ($< 5\%$ of the time), the center of mass will be positioned outside the region and these results will be neglected in the following.

Figure 8 shows an example of the wake center position relative to the hub location as function of time. Clearly, the lateral movement is larger and there are large fluctuations following a Strouhal frequency related to the spacing, see Andersen et al. [26].

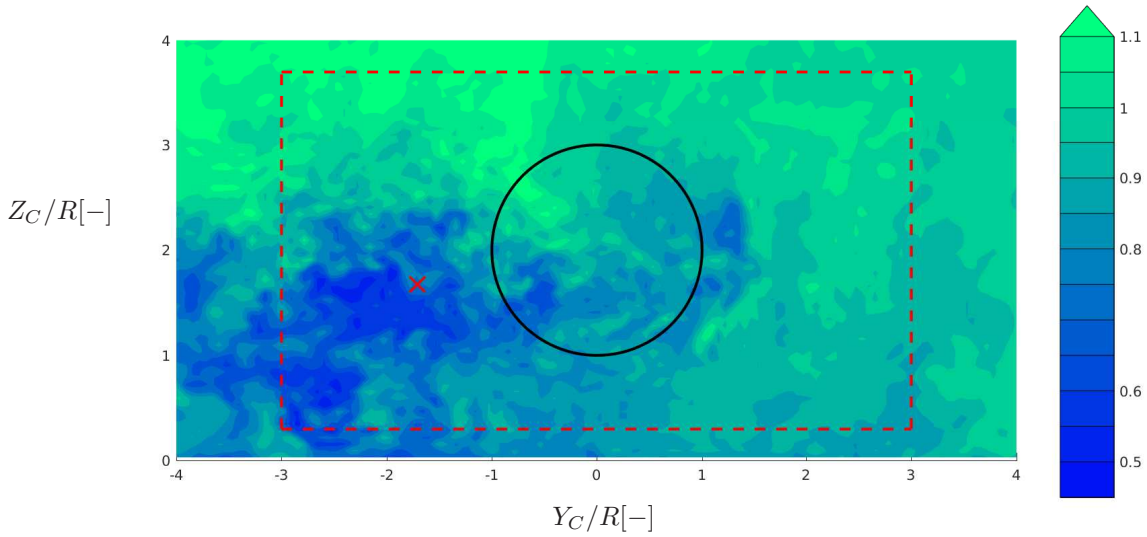

Figure 7. Illustration of wake center position marked by red "X" seen $11R$ behind upstream turbine. Contours show streamwise velocity, black circle is turbine area as seen from behind and red broken lines indicate search area.

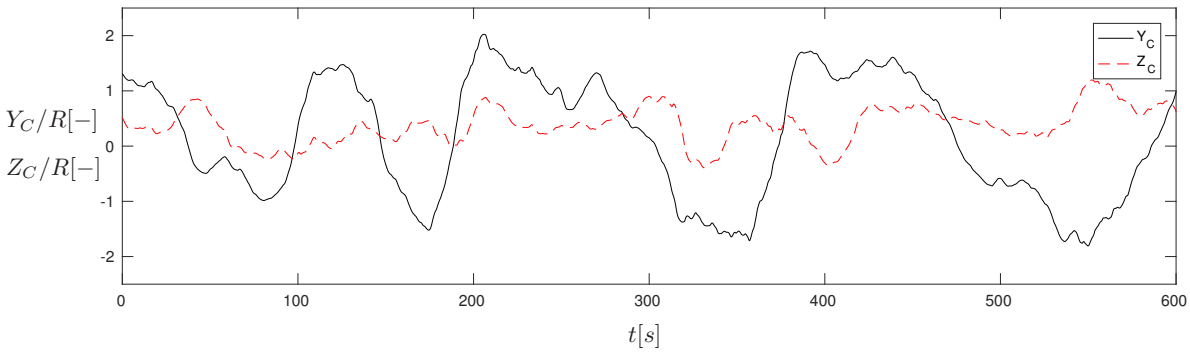

Figure 8. Time series of wake center position relative to hub location for turbine no. 11. Y_C (black) and Z_C (red) are lateral and vertical position, respectively.

Unlike, the yaw steering investigations performed by *e.g.* Gebraad et al. [8] and Fleming et al. [9], the turbine(s) are not intentionally yawed here. The turbines are aligned with the main wind direction, but as shown in Andersen et al. [27] the instantaneous wind direction varies significantly (more than $\pm 15°$) even within an aligned row of turbines. So these turbines experience unintentional and "unknown" yaw misalignment like real operating turbines. The question here is how correlated the dynamic wake position is to the turbine operation, which created the wake.

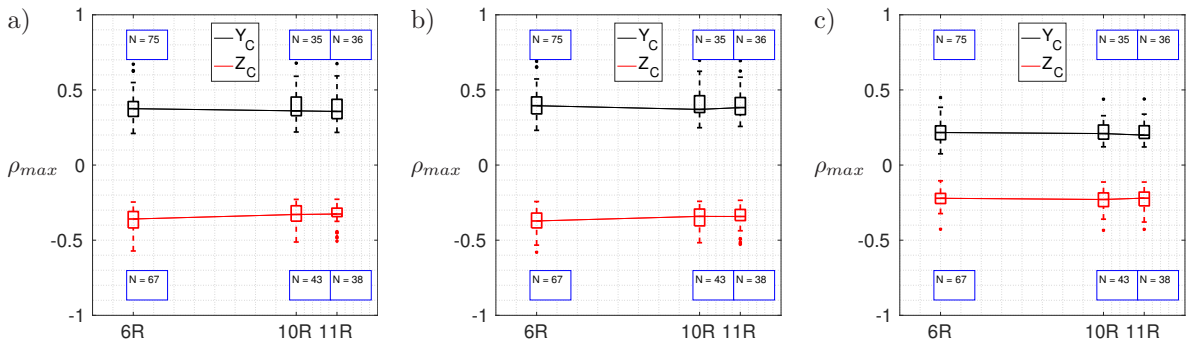

Figure 9. Boxplot of maximum correlation between the center of the wake (Y_C (black) and Z_C (red)) and a) thrust force, b) axial tower root bending moment, and c) lateral tower root bending moment. The results are based on wake flow and turbine response behind the 6th to 14th turbine in a row of 16 turbines. The thin lines connect the medians for the three different distances behind the turbine. The correlations for Z_C are plotted negative. N shows the number of 10min cases used for the boxplot.

The cross-correlation of the wake position and the turbine loads have been computed for the same 10min periods as previously. The results are summarised in the boxplots in Figure 9 in terms of thrust force and the axial and lateral tower root bending moment. The figure shows the distribution of the maximum cross-correlation for the three different distances behind each turbine, namely $6R$, $10R$, and $11R$. Notice, that the latter two might be influenced by the induction of the following turbine.

The median correlation between the thrust force and the horizontal wake position is just above 35% and a little less than 35% to the vertical wake position, and there is a very weak decreasing trend for increased distance from the turbine. Some outliers exist, but the spread in the quartiles are quite small. The thrust is directed axially, so the tower root bending moments in the axial and lateral direction are also shown. These moments are important structurally, but can in this context also be viewed as a proxy for yaw misalignment since a change in wind direction will result in an increased lateral tower root bending moment and a wake deflection. The axial tower root bending moment is directly related to the thrust, and hence shows very comparable correlations, *i.e.* in the order 35%. The lateral tower root bending moment are only correlated with the horizontal wake position by approximately 20% and perhaps surprisingly slightly higher (22%) to the vertical wake position. Similar correlations were seen for yaw and tilt loads (not shown for brevity).

The low correlations between the instantaneous turbine response and wake position is also discouraging. Wake steering also includes important dynamics of the wake movement, which should be considered to ensure that it does not result in additional half-wake scenarios for the following turbine. However, it should be emphasized that these results are dynamic results derived from unintentional yaw misalingment and not intentionally yaw misalignment, so further studies into the movement of the intentionally yawed wake would be necessary.

4. Conclusion

A long row turbines is modelled using large eddy simulations and the actuator line method coupled to the aero-elastic tool, Flex5. This provides time series of both flow as well as loads, deflections, and power production of each of the turbines. The mutual fluid-structure interaction and response is investigated in terms of temporal correlations throughout the flowfield surrounding each turbine as well as a more global comparison between the turbine loading and

the wake. The results give insights useful for how to perform dynamic control of individual turbines within large wind farms, when employing either induction-based, wake steering, or a combination or the two.

The correlation of the fluid-structure interaction is shown to be high and extend several radii upstream of the turbine. This can be utilized for instance by installing forward-facing lidars on the nacelle to measure the incoming wind directly for the controller, which requires a sufficiently precise measurement as well as ample time for the controller to correctly respond. However, the correlation between turbine and the wake flow is low. A high correlation between thrust and wake is not necessarily crucial for induction based control strategies, as it could potentially trigger a faster wake breakdown and recovery, hence a higher mean velocity and power production for the following turbine(s).

The correlation between the turbine and the wake position was shown to be low for unintentionally yaw misalignment. The surprisingly low correlations clearly showcase that the wake position is also highly dynamic. Hence, detailed and instantaneous knowledge of the inflow is crucial in order to intentionally and consistently steer wakes away from the following turbines. Otherwise, a control strategy based on steady considerations might end up exacerbating the loads on both the yawed turbines as well as on the following turbine by increasing the amount of half-wake situations rather than mitigating the overall wake effects.

4.1. Acknowledgments

The proprietary data for Vestas' NM80 turbine has been used. The work has been done as part of the CCA on High Fidelity Modelling and Virtual Atmosphere.

References

[1] Troldborg N and Meyer Forsting A 2017 *Wind Energy* **20** 2011–2020 ISSN 1095-4244
[2] Mann J, Peña A, Troldborg N and Andersen S J 2017 *Wind Energy Science Discussions* **2017** 1–13 URL https://www.wind-energ-sci-discuss.net/wes-2017-53/
[3] Jensen N O 1983 A note on wind generator interaction
[4] Bastankhah M and Port-Agel F 2017 *Physics of Fluids* **29** 18. 065105
[5] Sørensen J, Mikkelsen R, Henningson D, Ivanell S, Sarmast S and Andersen S 2015 *Phil. Trans. R. Soc. A* **373** ISSN 1364-503X
[6] Steinbuch M, de Boer W, Bosgra O, Peters S and Ploeg J 1988 *Journal of Wind Engineering and Industrial Aerodynamics* **27** 237 – 246 ISSN 0167-6105 URL http://www.sciencedirect.com/science/article/pii/0167610588900396
[7] Annoni J, Gebraad P M O, Scholbrock A K, Fleming P A and Wingerden J W v 2016 *Wind Energy* **19** 1135–1150 ISSN 1099-1824 we.1891 URL http://dx.doi.org/10.1002/we.1891
[8] Gebraad P M O, Teeuwisse F W, van Wingerden J W, Fleming P A, Ruben S D, Marden J R and Pao L Y 2016 *Wind Energy* **19** 95–114 ISSN 1099-1824 we.1822 URL http://dx.doi.org/10.1002/we.1822
[9] Fleming P, Annoni J, Churchfield M, Martinez L, Gruchalla K, Lawson M and Moriarty P 2017 *Wind Energy Science Discussions* **2017** 1–17 URL https://www.wind-energ-sci-discuss.net/wes-2017-52/
[10] Goit J and Meyers J 2015 *Journal of Fluid Mechanics* **768** 5–50
[11] Munters W and Meyers J 2018 *Wind Energy Science Discussions* **2018** 1–27 URL https://www.wind-energ-sci-discuss.net/wes-2018-15/
[12] Michelsen J A 1992 Basis3D – a Platform for Development of Multiblock PDE Solvers Tech. rep. Danmarks Tekniske Universitet
[13] Sørensen N N 1995 *General Purpose Flow Solver Applied to Flow over Hills* Ph.D. thesis Technical University of Denmark
[14] Sørensen J N and Shen W Z 2002 *J. Fluids Eng.* **124** 393–399
[15] Øye S 11-12 April 1996 (Lyngby, Denmark: Danmarks Tekniske Universitet) pp 71–76
[16] Aagaard Madsen H, Bak C, Schmidt Paulsen U, Gaunaa M, Fuglsang P, Romblad J, Olesen N, Enevoldsen P, Laursen J and Jensen L 2010 *The DAN-AERO MW Experiments* Denmark. Forskningscenter Risø. Risø-R (Danmarks Tekniske Universitet, Risø Nationallaboratoriet for Bæredygtig Energi)
[17] Andersen S J, Sørensen J N, Mikkelsen R and Ivanell S 2016 *Journal of Physics: Conference Series* **753** 032002 URL http://stacks.iop.org/1742-6596/753/i=3/a=032002
[18] Mikkelsen R, Sørensen J and Troldborg N 2007 *EWEC*

[19] Troldborg N, Sørensen J and Mikkelsen R 2009 *EWEC 2009 Proceedings online* (EWEC)
[20] Mann J 1994 *Journal of Fluid Mechanics* **273** 141–168 ISSN 1469-7645
[21] Mann J 1998 *Probabilistic Engineering Mechanics* **13** 269–282 ISSN 0266-8920
[22] Andersen S, Sørensen J and Mikkelsen R 2017 *Philosophical Transactions of the Royal Society A: Mathematical, Physical and Engineering Sciences* **375** 20160107–20160107 ISSN 1364-503X
[23] Borraccino A, Courtney M and Wagner R 2017 *Remotely measuring the wind using turbine-mounted lidars: Application to power performance testing* Ph.D. thesis Denmark
[24] Mirzaei M, Göçmen Bozkurt T, Giebel G, Sørensen P and Poulsen N 2015 *Turbine Control Strategies for Wind Farm Power Optimization* (IEEE) pp 1709 – 1714 ISBN 978-1-4799-8685-9
[25] Andersen S J 2013 *Simulation and Prediction of Wakes and Wake Interaction in Wind Farms* Ph.D. thesis Technical University of Denmark, Wind Energy.
[26] Andersen S J, Sørensen J N and Mikkelsen R 2013 *Journal of Turbulence* **14** 1–24 (*Preprint* `http://www.tandfonline.com/doi/pdf/10.1080/14685248.2013.796085`)
[27] Andersen S, Witha B, Breton S P, Sørensen J, Mikkelsen R and Ivanell S 2015 *Journal of Physics: Conference Series (Online)* **625** ISSN 1742-6596